Decentralized Load Sharing in a Low-Voltage Direct Current Microgrid With an Adaptive Droop Approach Based on a Superimposed Frequency

Peyghami, Saeed; Mokhtari, Hossein; Blaabjerg, Frede

Published in:
IEEE Journal of Emerging and Selected Topics in Power Electronics

DOI (link to publication from Publisher):
10.1109/JESTPE.2017.2674300

Publication date:
2017

Document Version
Accepted author manuscript, peer reviewed version

Decentralized Load Sharing in an LVDC Microgrid with an Adaptive Droop Approach Based on a Superimposed Frequency

Saeed Peyghami[1], *Student Member, IEEE,* Hossein Mokhtari[1], *Senior Member, IEEE,* and Frede Blaabjerg[2], *Fellow, IEEE*

***Abstract*— Conventional droop methods for load sharing control in Low Voltage Direct Current (LVDC) microgrids suffer from poor power sharing and voltage regulation, especially in the case when operating many dc sources with long feeders. Hence, the communication based approaches are employed to improve the load sharing accuracy and voltage regulation. To avoid using such an infrastructure and the corresponding effects on the reliability and stability, an adaptive droop controller based on a superimposed frequency is proposed in this paper. Load sharing accuracy is improved by adapting the droop gains utilizing an introduced ac-power. The secondary controller locally estimates and compensates the voltage drop due to the droop controller. The proposed power sharing approach can properly control the load sharing and voltage regulation without utilizing any extra communication system. The effectiveness of the proposed control system is verified by simulations and experimental tests.**

***Index Terms*— DC Microgrid, Droop Method, Frequency Injection, Adaptive Droop Control, Power Sharing.**

I. Introduction

THE concept of microgrid technology has been introduced in the last decade in order to improve the power system stability, reliability, and efficiency as well as to decrease the losses and operational costs. Although most studies have focused on ac microgrid, dc microgrid is becoming more popular due to its major advantages over the ac power system [1]–[3]. Most of the energy units including renewable energies and storages are commonly dc or have a dc coupling in their conversion stage. Also, electronic and power electronic loads can be operated by dc power. Meanwhile, eliminating the power conversion stages in full converter-based sources and variable speed drives will further reduces the expenses. Moreover, non-linear and reactive loads do not exist in dc systems, which in ac systems introduce power loss, lifetime reduction and etc. over the transformers, capacitors, and other equipment. Therefore, integrating dc sources, storages, and loads into a dc microgrid will enhance the overall performance of the system compared to the ac microgrid.

To control and operate dc based power grids, a suitable power management system is required. A hierarchical load sharing control system has been presented in three levels including primary, secondary, and tertiary controllers [4]–[11]. Tertiary controller is in charge of optimal power flow control in microgrids, which in most cases should be implemented by a low bandwidth communication network. Secondary controller also requires a communication network to regulate the voltage of the system within an acceptable region. Primary controller locally carries out resilient load sharing among different sources, generally by utilizing a virtual resistor as a droop controller.

A simple droop method is employed to properly control the load sharing among dc converters. In this approach, the line resistances are usually neglected, and the dc bus voltage is the same for all the converters [9], [12]–[14]. Therefore, with a small virtual resistor, an appropriate load sharing can be achieved. However, considering the line resistance effect, large virtual resistors should be utilized to carry out the appropriate load sharing. Large virtual resistors cause large voltage drop within the grid, which in most cases are compensated by employing a secondary control layer reinforced by a communication network. Point to point communication [8], [15] as well as sparse communication among converters [4], [6] are employed to reach the power management objectives including proportional load sharing and acceptable voltage regulation. However, the communication network may affect the stability and reliability of the system [4], especially in the case of operating many sources along long feeders.

Although less common, independence of communication is possible, as demonstrated in [16], where a load-sharing approach based on frequency encoding of output current of converters has been introduced. Another technique, named as power talk, has also been mentioned in [17], where sources in the dc microgrid "talk" to each other by modulating their respective power levels without using external communication links. The approach is however prone to line, load, and other grid parameter changes, which in practice, are unpredictable. Another frequency based control approach is presented in [18] for energy management purpose in dc microgrids without utilizing a communication network. However, the expandability of the system is limited due to the additional currents required by the converters to sustain a certain ac signal. Moreover, this approach is only suitable for energy management level which requires slow dynamic response, and hence it cannot be employed in primary control level. A frequency-based power sharing technique proposed in [19] and [20], and later reapplied to dc microgrids in [21], may

[1] Saeed Peyghami and Hossein Mokhtari are with the Department of Electrical Engineering, Sharif University of Technology, Iran (e-mail: saeed_peyghami@ee.sharif.edu, mokhtari@sharif.edu).

[2] Frede Blaabjerg is with the Department of Energy Technology, Aalborg University, Denmark (e-mail: fbl@et.aau.dk).

therefore be more appealing, since it is based on the same conventional droop principle, while yet ensuring very low affection towards variations.

In order to overcome the communication issues as well as to obtain the power sharing objectives, a frequency droop approach is introduced in [22]. Furthermore, this approach is generally analyzed and experimentally validated in [23]. Analogies of the frequency droop control between ac and dc microgrids are also studied in [23]. However, the stability of the frequency droop control in terms of load variation is questionable. In order to improve the overall system stability, in this paper a new adaptive droop approach based on a frequency injection method merged with a virtual resistor is proposed. In the proposed approach, both primary and secondary controllers locally carry out the load sharing and the voltage regulation without utilizing communication network, which leads to reliable and stable operation. The remaining part of this paper is organized as follows. After a short explanation of the conventional load sharing approach in Section II, the proposed adaptive droop controller as well as the small signal stability analysis is presented in Section III. The obtained simulation results and experimental validations are reported in Section IV and V respectively. Finally, the outcomes of the paper are summarized in Section VI.

II. Conventional Load Sharing Approach

In a dc microgrid, the load sharing among different converters depends on the line resistances. As it is shown in Fig. 1, considering the same voltage for both converters ($V_{o1} = V_{o2}$), the output current is inversely proportional to the line resistances (i.e., $I_{o2}/I_{o1} = R_1/R_2$), where I_{o1} and I_{o2} are the output current of converters and R_1 and R_2 are the corresponding line resistances. This load sharing based on the line resistances may cause overstress of the converters.

Therefore, a load sharing approach needs to be applied to adjust the output voltage of the converters, and hence, to control the output current of them. The most common used load sharing method is a droop controller [9], [12]–[14], which is explained in the following.

A. Conventional Droop Control Approach

Droop controller is a reliable and resilient approach for load sharing control in dc microgrids, and as a primary load sharing method, it locally determines the reference current of each converters by employing the output current and/or voltage. As shown in Fig. 2, the primary droop controller of the k^{th} converter adapts the set point of the inner voltage regulator utilizing a virtual resistor R_{dk} multiplied by the output current (I_{ok}). Considering the simplified microgrid shown in Fig. 1, the output current and voltage of converters employing the droop controller can be found by solving (1) and (2) as:

$$\begin{cases} V_{o1} = V_{PCC} + R_1 I_{o1} \\ V_{o2} = V_{PCC} + R_2 I_{o2} \end{cases}, \quad (1)$$

$$\begin{cases} V_{o1} = V^* - R_{d1} I_{o1} \\ V_{o2} = V^* - R_{d2} I_{o2} \end{cases}, \quad (2)$$

where V^* is the nominal voltage of the microgrid. This can be graphically determined as shown in Fig. 3 (a) for small and large droop gains $R_{ds} > R_{dl}$. As it can be seen from Fig. 3 (a), the mismatch between the output currents in the case of larger droop gain R_{d2} is smaller than that of the smaller droop gain R_{d1} (i.e., $\Delta I_1 < \Delta I_2$). However, increasing the droop gain causes a larger voltage drop. As it can be seen from Fig. 3 (a), the voltage drop of the larger droop gain is higher than the voltage drop of the smaller one (i.e., $\Delta V_1 < \Delta V_2$).

Therefore, improving the current sharing accuracy deteriorates the voltage regulation [4], [8]. In order to achieve the accurate load sharing, large droop gains can be used, and hence to restore the voltage drop due to the large droop gains, a secondary control layer is employed as shown in Fig. 2, which is explained in the next subsection.

B. Secondary Control

A secondary controller restores the voltage drop of the primary controller as shown in Fig. 2. It can be implemented in either a central approach or a distributed methods. In the centralized approach the voltage at the coupling point of the load or local grid is measured and regulated by a controller [4], [8]. The output of the central controller, as a restoration term $\delta_{v,k}$, is sent to all of the units to shift up their droop characteristics as shown in Fig. 3 (b). To implement the central voltage regulator, a communication network is required between the central controller and converters, which affects the reliability and stability. To improve the overall reliability and stability, some decentralized approaches are represented [6], [24]. In these approaches, sparse communication among the neighboring converters is employed, and a dynamic consensus protocol based control algorithm guarantees the voltage regulation in the microgrid.

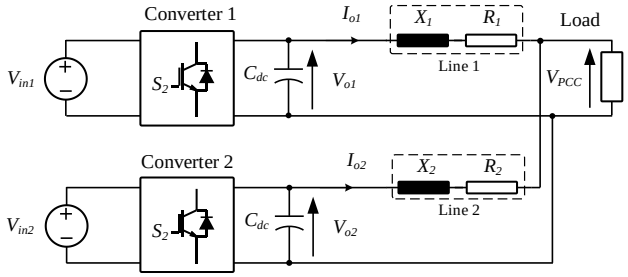

Fig. 1. Simplified dc microgrid with two DGs and a localized load.

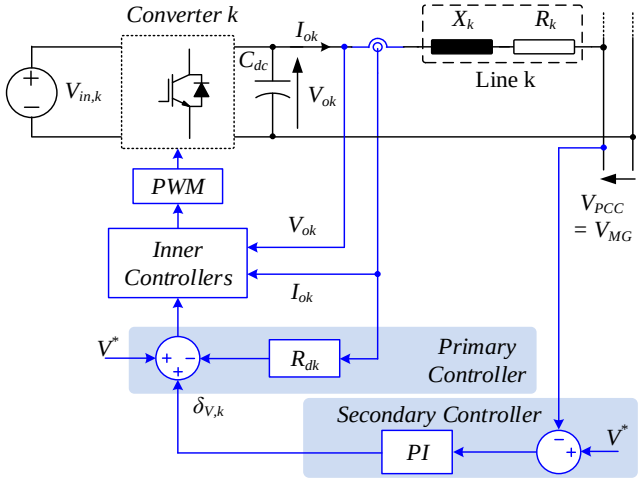

Fig. 2. Schematic and control block diagram of a primary and secondary controller for the k^{th} converter in a dc microgrid – (V_{MG}: Microgrid Voltage also called V_{PCC}).

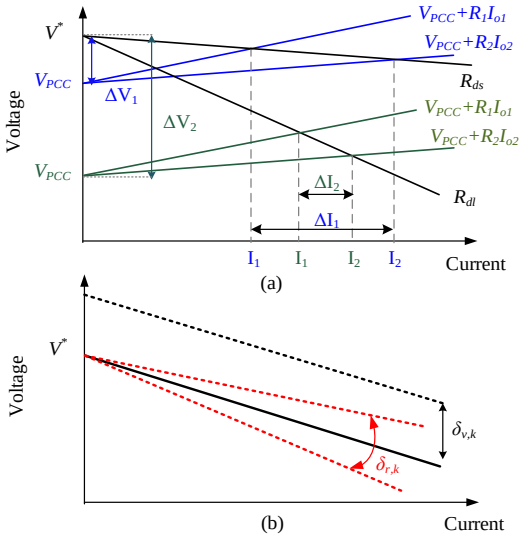

Fig. 3. Conventional droop characteristics for dc sources in a dc microgrid: (a) effect of different droop gains, (b) effect of secondary controller.

However, load sharing cannot be accurately performed by increasing the droop gains, and stability issues may occur using higher droop gains. Therefore, some average current regulators and circular chain controllers are presented in [25]–[29] to increase the sharing accuracy. In fact, these methods regulate the per unit output current of the converters by adapting the slope of the droop characteristics as shown in Fig. 3 (b), where $\delta_{r,k}$ is the output of the average current regulator. This correction term adjusts the droop slope such that the appropriate load sharing is achieved.

Both voltage and current regulators in secondary layer require communication of the current and voltage information among the converters. To avoid such an infrastructure and its accompanied complications as well as to improve the reliability and stability of the system, in the next section, a proposed load sharing approach without a communication network is presented.

III. Proposed Load Sharing Approach

The proposed control system based on a superimposed frequency shown in Fig. 4, including conventional droop controller, an ac signal generator, adaptive droop controller, and a secondary controller. Conventional droop control is discussed in the last section. Ac signal generator superimposes a small ac voltage onto the dc voltage to be modulated by the switching converter. The adaptive droop control carry out the accurate load sharing between the converters by adjusting the conventional droop gains, and the secondary controller compensates the voltage drop due to the conventional droop gain. The proposed control system is explained in the following.

A. AC Signal Generator

To ensure appropriate load sharing between converters, a small ac voltage is superimposed onto the output dc voltage by each converter. The frequency of the injected ac voltage is proportional to the output dc current of the converter, which can be defined as:

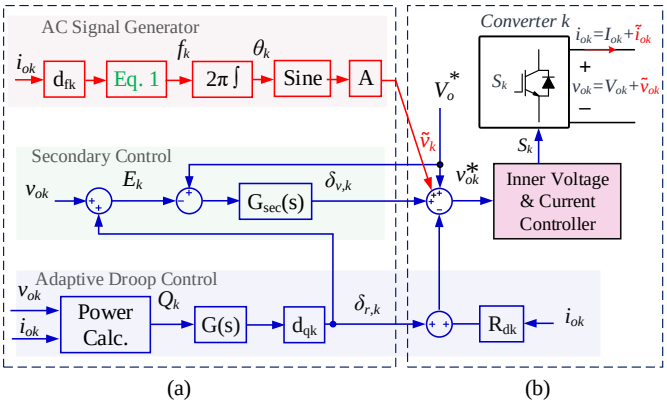

Fig. 4. Block diagram of the proposed control system, (a) adaptive controller, and (b) conventional droop controller.

$$f_k = f^* - d_{fk} i_{ok} \ , \tag{3}$$

where f^* and f_k are the rated and injected frequency, i_{ok} is the output current and d_{fk} is the frequency droop gain, and k denotes the k^{th} converter. The injected frequency should be smaller than the bandwidth of the inner voltage controller to be properly generated by the converter.

The injected ac voltage causes ac current flow in the microgrid which is proportional to the phase angle (θ_k) of the ac voltages as well as the line impedances. According to Fig. 4 (a), the phase angle of the ac voltage of the k^{th} converter can be found as:

$$\theta_k(t) = \int_{\tau=0}^{t} 2\pi f_k d\tau \ . \tag{4}$$

Considering the same ac voltage magnitude denoted as A, and the load impedance is higher than the line impedances, the ac current flowing between the converters $\tilde{i}_{o1}$ and $\tilde{i}_{o2}$ can be calculated as:

$$\tilde{i}_{o1} \approx \frac{A\angle\theta_1 - A\angle\theta_2}{R_1 + R_2 + j(\mathrm{X}_1 + \mathrm{X}_2)} = -\tilde{i}_{o2} \tag{5}$$

If the injected frequency is low enough, the line reactance can be neglected [30]. Therefore, the ac current can be found as:

$$\tilde{i}_{o1} \approx \frac{A\angle\theta_1 - A\angle\theta_2}{R_1 + R_2} = -\tilde{i}_{o2} \tag{6}$$

According to (6), the ac currents contain the information of voltage phases as well as line resistances. On the other hand, phase angles are proportional to the output currents of the converters based on (3). Therefore, the ac currents can be used to make a communication between the converters, without extra communication equipment. As a result, considering the same frequencies for the converters at steady state, the ratio of the output current of the converters (ξ) based on (3) can be calculated as:

$$\frac{i_{o1}}{i_{o2}} = \frac{d_{f2}}{d_{f1}} = \xi \ . \tag{7}$$

Therefore, the output currents of the converters can be shared inversely proportional to the desired droop gains. This concept has been used in droop controlled ac microgrids, where the active power of inverters can be controlled by employing a common frequency of the microgrid [15], [28], [31]–[34]. Here, in the dc microgrid, to reach the same frequency for the converters, it is required to control an ac power. On the other hand, in LV systems, the reactive power

can be controlled by the frequency [30], [35], [36]. Hence, the reactive power shared between the converters, can be used to reach the same frequency in the grid, which introduces a proper current sharing based on (7). The injected reactive power is used to adapt the conventional droop gains in order to achieve the proportional load sharing. The adaptive control approach is explained in the following.

B. Adaptive Droop Controller

The ac reactive power is proportional to the ac currents and hence the phase angles. Furthermore, the phase angles are related to the dc currents, which can also be controlled by the dc voltages. Therefore, adjusting the dc voltages based on the reactive power can control the output dc current.

Considering the load impedance higher than the line impedances, the ac reactive power (Q_1, Q_2) is only flowed between converters and can be calculated as:

$$Q_1 = -Q_2 = \frac{A^2}{2(R_1 + R_2)} Sin(\theta_1 - \theta_2) \ , \tag{8}$$

where Q_k, θ_k, and R_k are the reactive power, voltage angle and line resistance of the k^{th} converter. Therefore, according to Fig. 4, the dc voltage reference can be modified as:

$$\begin{aligned} v_{ok}^{*} &= V^{*} - R_{dk} i_{ok} + \delta_{r,k} \\ \delta_{r,k} &= d_{qk} G(s) Q_k \end{aligned} \ , \tag{9}$$

where d_{qk} is the voltage coupling gain, and $G(s)$ is a first order low pass filter to attenuate the high frequency components of the calculated reactive power. Also, R_{dk} denotes the conventional droop gain (virtual resistor) and it can be defined as:

$$R_{dk} = \frac{\Delta V}{I_{n,k}} \ , \tag{10}$$

where ΔV is the maximum allowable dc voltage deviation, and $I_{n,k}$ is the nominal current of the k^{th} converter. Therefore, the relationship between the output current of converters (I_1, I_2) at the steady state can be found as:

$$\frac{I_1}{I_2} = \frac{I_{n,1}}{I_{n,2}} = \frac{R_{d2}}{R_{d1}} = \xi \ . \tag{11}$$

The equation (9) can be rearranged as:

$$v_{ok}^{*} = V^{*} - R_{dk} i_{ok} + \frac{d_{pk} G(s) Q_k}{i_{ok}} i_{ok} \ , \tag{12}$$

$$v_{ok}^{*} = V^{*} - R_{dk} i_{ok} \ , \tag{13}$$

where R_{dk} is the resultant droop gain of k^{th} converter, and it can be adapted based on corresponding loading conditions and can be defined as:

$$R_{dk} = R_{dk} + \frac{d_{pk} G(s) Q_k}{i_{ok}} \ . \tag{14}$$

Therefore, the conventional droop gain can be adapted in order to reach an acceptable load sharing between the converters as it is graphically shown in Fig. 3 (b).

The conventional droop gain introduced in [9], [12]–[14] includes the first term of (14). Hence the load sharing accuracy is not precise. Therefore, communication based approaches are presented in order to improve the sharing accuracy [4], [8]. Moreover, in [22], [23], a frequency based droop approach is introduced which only includes the second term of (14). According to [22], [23], the sensitivity of the droop gain to load variation is very high, thus, affecting the stability of the system. However, in the proposed approach the droop controller is comprised of two terms of an adaptive part and a fixed part as given in (14), enhancing the system stability. Employing the fixed term causes the voltage drop in the microgrid which can be compensated by a secondary control. In the following, the proposed decentralized secondary approach is presented.

C. Decentralized Secondary Control

Defining the variable term of droop gain in (14) as:

$$r_{dk} := \frac{d_{pk} G(s) Q_k}{i_{ok}} \ , \tag{15}$$

the steady state electrical model of the system can be represented as shown in Fig. 5. The system model contains conventional droop gain (virtual resistor), adaptive droop gain, and line resistor. From the electric circuit theory, the internal voltage of each converter denoted by E_k in Fig. 5, can be found as:

$$\begin{cases} E_1 = V^{*} - R_{d1} I_1 \\ E_2 = V^{*} - R_{d2} I_2 \end{cases} \tag{16}$$

Based on (11), the voltage drops on the virtual resistors (R_{d1},R_{d2}) at the steady state are equal, and hence, according to (16), the internal voltage of both converters are the same. Therefore, it can be estimated and regulated by the secondary regulator to compensate the voltage drop due to the droop gains. By measuring the output voltage (v_{ok}) and calculating the adaptive correction term ($\delta_{r,k}$), the internal voltage (E_k) can be found as:

$$E_k = v_{ok} + \delta_{r,k} \ . \tag{17}$$

Therefore, the secondary correction term ($\delta_{v,k}$) can be generated by a PI controller ($G_{sec}(s)$) to regulate the internal voltage at the reference value as:

$$\delta_{v,k} = (V^{*} - E_k) G_{sec}(s) \ . \tag{18}$$

According to Fig. 4, the reference voltage of the k^{th} converter can be calculated as:

$$v_{ok}^{*} = V^{*} + \delta_{v,k} - \delta_{r,k} - R_{dk} i_{ok} \ . \tag{19}$$

Considering the fast dynamics for the internal voltage and current loops in comparison to the secondary layer, the output voltage of the converter can properly track the reference value, and hence,

$$v_{ok}^{*} = v_{ok} = V^{*} - \frac{1}{1 + G_{sec}(s)} R_{dk} i_{ok} - d_q G(s) Q_k \ . \tag{20}$$

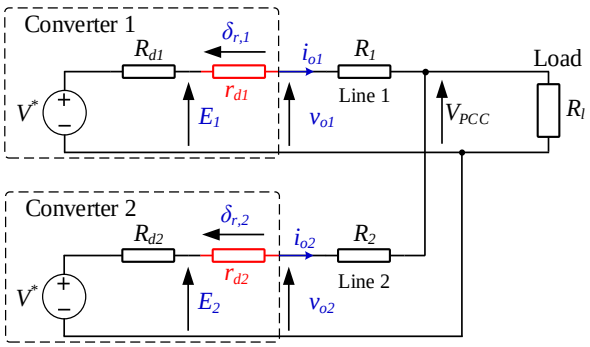

Fig. 5. Simplified dc MG with two DGs and a localized load.

As it can be seen in (20), the conventional droop resistor effect will be canceled at the steady state by the secondary PI regulator ($G_{sec}(s)$), since the term $1/(1+G_{sec}(s))$ in (20), is very small at low frequencies. Therefore, the voltage drop on the droop resistor can be compensated by the decentralized secondary regulator employing the local voltage and current information.

In the presence of converter based loads, the input capacitor of the converter consumes a reactive power, which is very small due to the low ac voltage and frequency. This reactive power needs to be supplied by one or more sources, and hence the r_{dk} in (15) is not equal for the source converters. Since the reactive power consumption by the load capacitors is small, it cannot affect the voltage regulation unlike the conventional droop approaches. However, in the case of very large dc capacitors of loads, the performance of the control system may be limited. In this case, the control system may be redesigned to reduce the effect of capacitors' reactive power consumption on the voltage regulation by reducing the injected frequency, and/or reducing the voltage–power coupling gain and increasing the virtual resistor to have an appropriate dynamic response as well as small voltage regulation error. Furthermore, the effect of injected ac voltage on the converter based constant power loads behavior are explained in the Appendix.

D. Dynamic Stability

In order to ensure the stability of the control system as well as to design the control system parameters, a small signal model of the system is established. Considering $\Delta(x)$ as a small variation of variable x, the linear form of (20) can be obtained as:

$$\Delta v_{ok} = -\frac{1}{1+G_{sec}(s)} R_{dk}\Delta i_{ok} - d_q G(s)\Delta Q_k \ . \qquad (21)$$

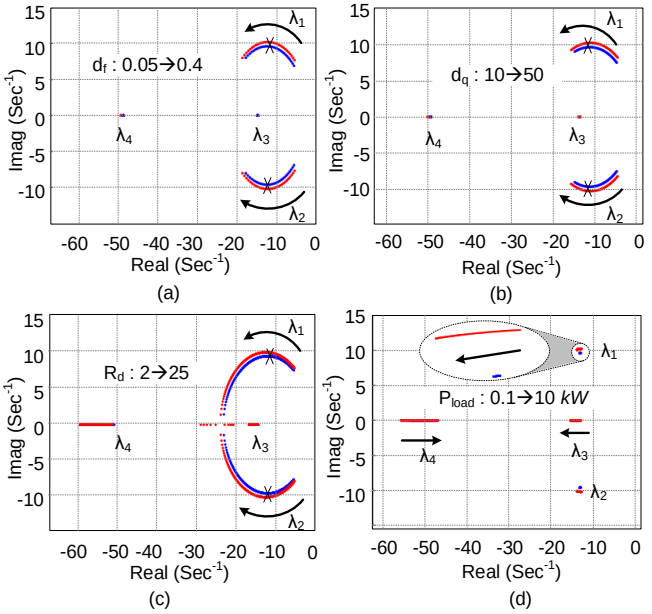

Fig. 6. Closed loop dominant place of system poles (λ_i denotes i^{th} pole): (a) effect of frequency droop gain; d_q = 25, R_d = 5, P_{load} = 2 *kW*, (b) effect of voltage-power coupling gain; d_f = 0.3, R_d = 5, P_{load} = 2*kW*, (c) effect of conventional droop gain; d_q = 25, P_{load} = 2 *kW*, and (d) effect of load variation; d_f = 0.3, R_d = 5 d_p = 25. – (blue: ξ = 1, and red ξ = 2). – Desired pole places for λ_1 and λ_2 are depicted by *X*, for R_d = 5, d_f = 0.3, P_{load} = 2 *kW*, d_q = 25, and ξ = 1, 2.

According to (8), the small variation of the ac reactive power can be calculated as:

$$\Delta Q_1 = -\Delta Q_2 = k_\delta \Delta(\theta_1 - \theta_2)$$
$$k_\delta = \frac{A^2}{2(R_1+R_2)} \ . \qquad (22)$$

Considering the relative angle of the injected voltage ($\theta = \theta_1 - \theta_2$) as a state variable, the linear form of (3) and (4) can be defined as:

$$\Delta\theta = \Delta(\theta_1 - \theta_2) = \frac{2\pi}{s}(d_{f2}\Delta i_{o2} - d_{f1}\Delta i_{o1}) \ . \qquad (23)$$

Furthermore, based on the equivalent electric circuit of the system shown in Fig. 5, the small signal model of the output voltage can be calculated as:

$$\begin{cases} \Delta v_{o1} = (R_1+R_l)\Delta i_{o1} + R_2\Delta i_{o2} \\ \Delta v_{o2} = R_1\Delta i_{o1} + (R_2+R_l)\Delta i_{o2} \end{cases}, \qquad (24)$$

where R_l is the load resistance. Combining (21) to (24), the characteristic equation $\Phi(s)$ of the system can be calculated as:

$$\Phi(s) = 1 + \frac{2\pi}{s} df\left(\frac{G(s)d_q k_\delta}{\rho_1\rho_2 - R_l^2}\right)\times \left(\xi\rho_1 + \rho_2 + R_l(\xi+1)\right), \qquad (25)$$

where,

$$\begin{cases} \rho_1 = \left(R_1 + R_l + \dfrac{R_{d1}}{G_{sec}(s)}\right), \\ \rho_2 = \left(R_2 + R_l + \dfrac{R_{d2}}{G_{sec}(s)}\right). \end{cases} \qquad (26)$$

The dominant closed loop pole places of the system shown in Fig. 1, can be obtained by (25), and they are illustrated in Fig. 6. The effects of the frequency droop gain (d_f), voltage coupling gain (d_q), and conventional droop gain (R_d) on the closed loop pole places are shown in Fig. 6 (a), (b) and (c) respectively. The blue graph shows the poles of the system with equal converter ratings (ξ = 1) and the red one is related to the unequal converter ratings (ξ = 2). The designed control parameters are given in Table I, and shown by "x" in Fig. 6. The effect of load variation on the closed loop poles with the designed control parameters, is shown in Fig. 6 (d), where the load is varying from 0.1 *kW* to 10 *kW*. As it can be seen, the system still remains stable at a wide range of load variation, and dominant poles are not extremely affected by the load variation.

IV. Simulation Results

In order to demonstrate the performance of the proposed control system, a simplified dc microgrid with two converters, like the one shown in Fig. 1 is considered. Without losing the generality, conventional boost topologies are considered. The control parameters and converter specifications are given in Table I. Meanwhile, since the bandwidth of the voltage controller is 900 Hz, the injected frequency is considered as 50 Hz to be properly generated by the converters.

The effectiveness of the power sharing approach is verified with three case studies. In Case I, equal converter ratings are considered, and in Case II, the rating of the second converter is considered to be two times the first one. In Case III, the performance of the control system is demonstrated in presence of a dc motor supplied through a dc/dc converter.

The simulation results of Case I and Case II are depicted in Fig. 7 and Fig. 8. In both cases, a 1.3 *kW* and a 1 *kW* load are connected at t = 0.5 *Sec* and t = 2 *Sec* respectively. As it can be seen from Fig. 7 (a), the load is equally shared between two converters and the output current has the same value. Furthermore, due to the ac signal injection, a small ac ripple is superimposed onto the dc currents. The instantaneous current waveform are also illustrated in Fig. 7 (a) at t = 1.3 *Sec*, where the 180° phase difference between the ac currents indicates the ac power flows between the two converters. The voltage waveforms of the converters shown in Fig. 7 (b), illustrate an acceptable voltage regulation within the microgrid. The dc voltage of the converters is settled close to 400 *V*. Furthermore, the instantaneous voltage waveforms are shown at t = 1.3 *Sec*, with a 2.5 *V* sinusoidal ripple. The frequency of the superimposed ac voltage is shown in Fig. 7 (c), where the frequency is decreased by increasing the load.

Load sharing results between the two converters with different power ratings are also shown in Fig. 8. As shown in Fig. 8 (a), the output current of the first converter is two times that of the second one, since the capacity of the first converter is two times more than the second one. The output voltage of the converters is also regulated near to the reference value as shown in Fig. 8 (b). The variation of the injected frequency is also shown in Fig. 8 (c).

TABLE I
Specifications of the DC microgrid and control system – $\omega^* = 2\pi f^*$

Definition		Symbol	Case I	Case II	Case III
Injected frequency		f^* *(Hz)*	50	50	50
Frequency-current droop		d_{f1}, d_{f2} d_{f3} *(Hz/A)*	0.3, 0.3	0.3, 0.6	0.3, 0.3, 0.6
Superimposed ac voltage		*A (V)*	2.5	2.5	2.5
Voltage-power coupling		d_q *(V/VAR)*	25	25	25
DC link voltage		V_{dc} *(V)*	400	400	400
Inner controllers		*Voltage controller*	0.45 + 20 /s		
		Current controller	0.05 + 2/s		
Secondary regulator		*Voltage regulator*	0.88 + 8.6/s		
Loads		P_{load} *(kW)*	1, 1.3		4
DC Motor	Mechanical speed	ω_m*(rad/Sec)*	150		
	Mechanical torque	T_m *(Nm)*	27		
	Rotor Inertia	*J (Nms²)*	0.0881		
	Armature impedance	R_a *(Ω),* L_a*(H)*	0.57, 0.0046		
	Field impedance	R_f*(Ω),* L_f *(H)*	190, 0.2		
	Electrical Power	*P (kW)*	4		
Impedance of line 1		$r_1+j\omega^*L_1$ *(Ω)*	2+j0.0565		
Impedance of line 2		$r_2+j\omega^*L_2$ *(Ω)*	1.5+j0.0565		
Converter Parameters		*Ldc (mH)*	2		
		Cdc (μF)	500		

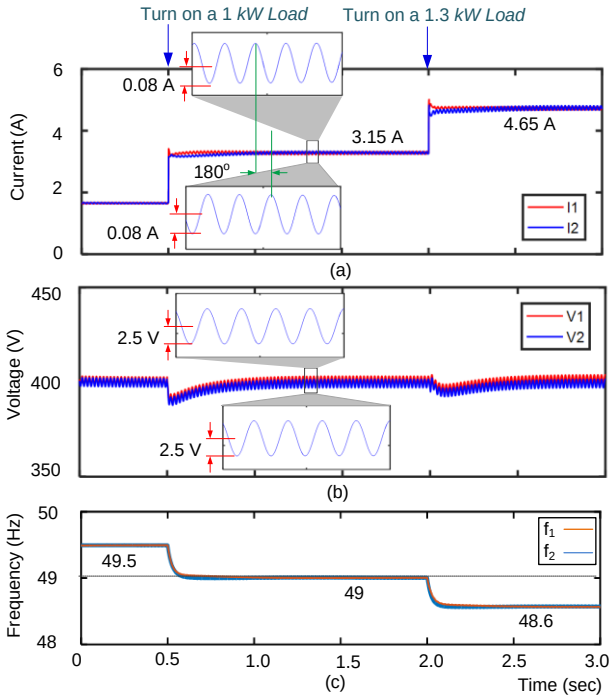

Fig. 7. Simulation results of Case I (see Table I) with the equal converter ratings, output current of (a) first and (b) second converters, output voltage of (c) first and (d) second converters, and (e) injected frequency.

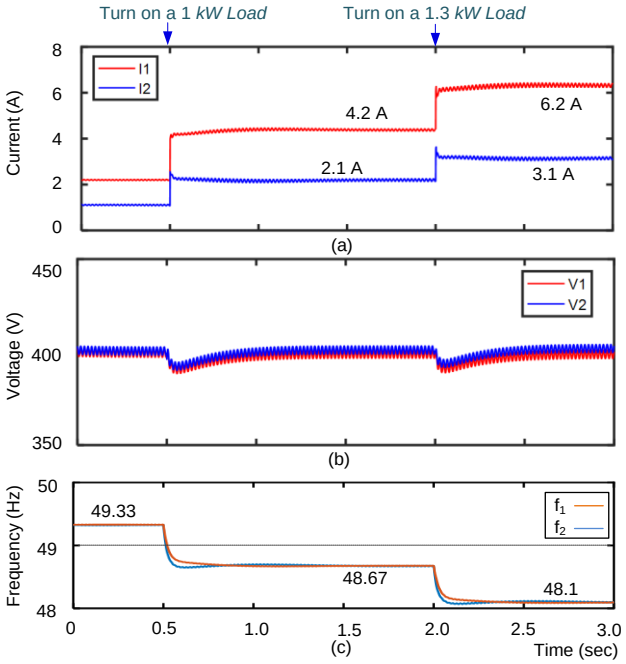

Fig. 8. Simulation results of Case II (see Table I) with unequal converter ratings, output current of (a) first and (b) second converters, output voltage of (c) first and (d) second converters, and (e) injected frequency.

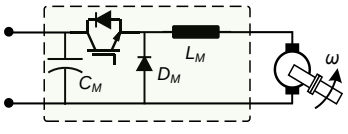

Fig. 9. Block diagram of the simplified dc motor-based constant power load – C_M = 200 *μF*, L_M = 2 *mH*.

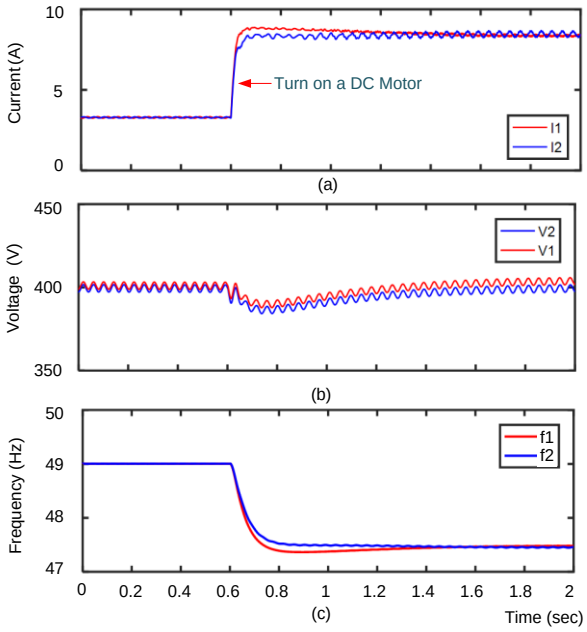

Fig. 10. Simulation results for Case III (see Table I), A 4 *kW* dc motor-based constant power load is connected at t = 0.6 *Sec*, V^* = 400 *V*.

In Case III, a dc motor is connected to the microgrid through a dc/dc converter shown in Fig. 9. The load and system parameters are given in Table I. At first, the converters are supporting a 2.7 kW load. At t = 0.6 *Sec*, the dc motor as a constant power load– with 27 *Nm* and 150 *rad/Sec* mechanical load – is connected to the microgrid. The output currents of converters are shown in Fig. 10(a) implying a proper load sharing in the presence of a converter-based constant power load. Furthermore, as shown in Fig. 10(b), the output voltage of converters is regulated close to the reference value after connecting the motor. The injected frequencies variations are also shown in Fig. 10(c).

The simulation results indicate an accurate load sharing between converters as well as an acceptable voltage regulation within the microgrid. Both primary and secondary controllers are employing the local grid information to reach the power sharing objectives. Further validations by experimental tests are given in the next section.

V. Experimental Results

In order to further validate the proposed method, some experimental tests are performed taking into consideration the load variations as well as equal and unequal converter ratings and different line impedances. The experimental setup shown in Fig. 11 contains two conventional boost converters with the parameters given in Table I. Each converter is controlled by its own Digital Signal Processor (DSP). The experimental results are reported in the following.

At first, the same ratings for both converters are considered, and the performance of the proposed adaptive droop is compared with the conventional droop method. The output current and voltage of the converters employing the conventional droop method are shown in Fig. 12. As it can be seen from Fig. 12, the output voltage of the converters is not regulated to the reference value and the load current is not equally shared between the two converters. Furthermore, by increasing the load, the output voltage drops and current mismatches are increased. However, utilizing the proposed control system gives an accurate current sharing between the converters as shown in Fig. 13. Moreover, after increasing the load from 1.2 *kW* to 1.7 *kW*, the dc voltages can be properly regulated close to the reference value, and hence the performance of the decentralized secondary controller can be further validated. Moreover, the ac ripple of the voltage and currents are 2.5 *V* and 0.1 *A* respectively.

The experimental results of power sharing for the unequal converter ratings are illustrated in Fig. 14 and Fig. 15 for $I_{n,1} = 0.5 \times I_{n,2}$ and Fig. 16 for $I_{n,1} = 2 \times I_{n,2}$. As it can be seen, the load is accurately shared between the converters and the dc voltage is properly regulated close to the reference value. As shown in Fig. 14, the output current of the second converter is two times that of the first one (R_1 = 1.5 Ω, R_2 = 2 Ω). After a load variation at t = 0.5 *Sec*, the load sharing is still accurately carried out and the voltage is regulated at the nominal value. To further evaluate the proposed controller, the line resistances are changed (i.e., R_1 = 2 Ω, R_2 = 1.5 Ω), and the results are shown in Fig. 15, implying an accurate load sharing and a proper voltage regulation.

Moreover, in the results shown in Fig. 16, the rating of the converters is changed and the performance of the proposed controllers are demonstrated in terms of sudden load reduction. As it can be seen, the output current of the first converter is two times that of the second one. In addition, the voltage can be restored after a load variation, and hence, the decentralized secondary controller can properly carry out the voltage regulation.

In the next test, the proposed adaptive frequency droop approach are compared with the frequency droop approach introduced in [22]. Power sharing between the two converters employing the frequency droop controller is shown in Fig. 17(a). As it can be seen in Fig. 17(a), the output currents of converters do not converge and the system is unstable. However, applying the adaptive frequency droop approach merged by the virtual resistor can properly control the power sharing between the two converters as shown in Fig. 17(b).

Finally, the synchronization procedure is shown in Fig. 18, where the second converter is initially turned on, and at t = 0.1 *Sec*, the first converter is connected. At t = 0.12 *Sec*, the PLL of the first converter extracts the phase of ac voltage and the second converter, injects the ac voltage. Therefore, both converters are properly synchronized and the currents are shared between the converters.

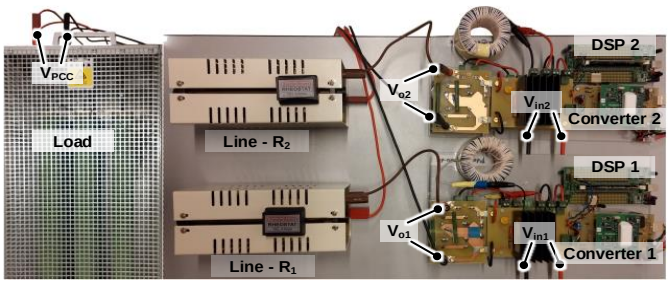

Fig. 11. Photograph of the implemented hardware setup based on two boost converters P_{load} = 1.2 + 0.5 *kW*.

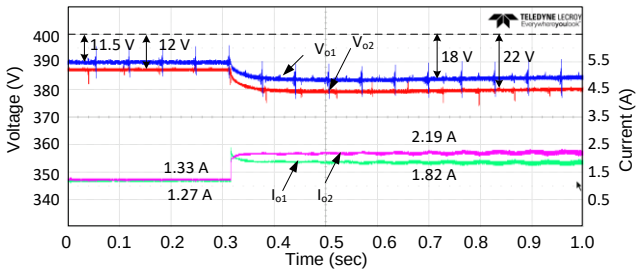

Fig. 12. Experimental results of conventional droop approach with equal converter ratings, $I_{n,1} = I_{n,2}$, $R_{d1} = R_{d2} = 10\ \Omega$, $R_1 = 2\ \Omega$, $R_2 = 1.5\ \Omega$, and $V^* = 400\ V$.

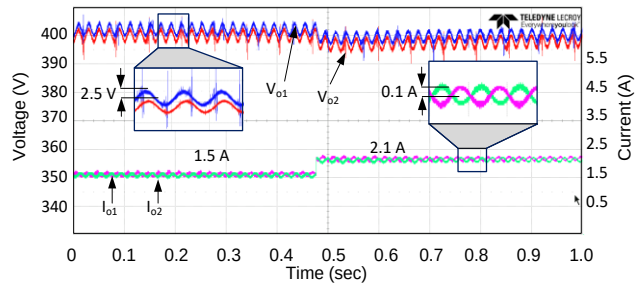

Fig. 13. Experimental results of adaptive droop approach with equal converter ratings, $I_{n,1} = I_{n,2}$, $d_{f1} = d_{f2} = 0.3$, $d_q = 25$, $R_{d1} = R_{d2} = 5\ \Omega$, $R_1 = 2\ \Omega$, $R_2 = 1.5\ \Omega$, and $V^* = 400\ V$.

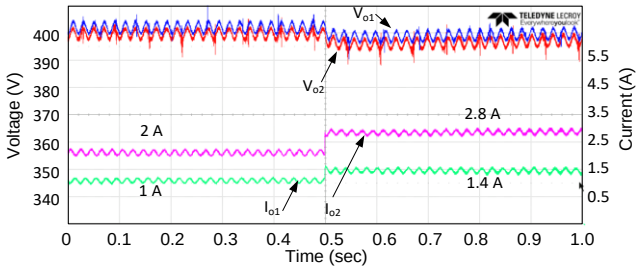

Fig. 14. Experimental results of adaptive droop approach with unequal converter ratings, $I_{n,1} = 0.5 \times I_{n,2}$, $d_{f1} = 2 \times d_{f2} = 0.6$, $d_q = 25$, $R_{d1} = 2 \times R_{d2} = 10\ \Omega$, $R_1 = 2\ \Omega$, $R_2 = 1.5\ \Omega$, and $V^* = 400\ V$.

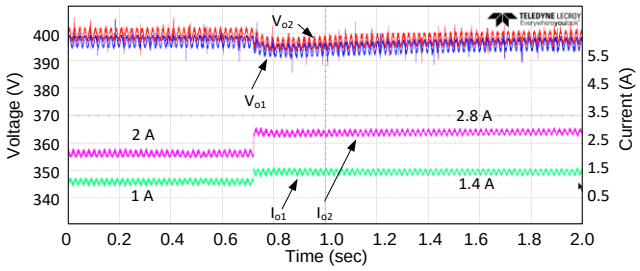

Fig. 15. Experimental results of adaptive droop approach with unequal converter ratings, $I_{n,1} = 0.5 \times I_{n,2}$, $d_{f1} = 2 \times d_{f2} = 0.6$, $d_q = 25$, $R_{d1} = 2 \times R_{d2} = 10\ \Omega$, $R_1 = 1.5\ \Omega$, $R_2 = 2\ \Omega$, and $V^* = 400\ V$.

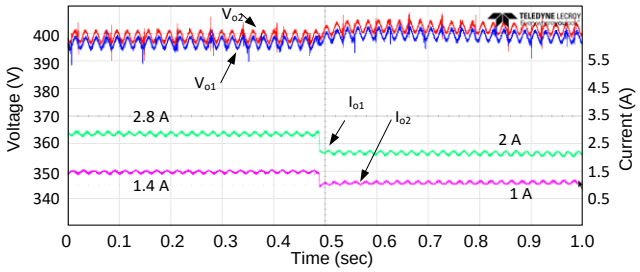

Fig. 16. Experimental results of adaptive droop approach with unequal converter ratings, $I_{n,1} = 2 \times I_{n,2}$, $d_{f1} = 0.5 \times d_{f2} = 0.3$, $d_q = 25$, $R_{d1} = 0.5 \times R_{d2} = 5\ \Omega$, $R_1 = 1.5\ \Omega$, $R_2 = 2\ \Omega$, and $V^* = 400\ V$.

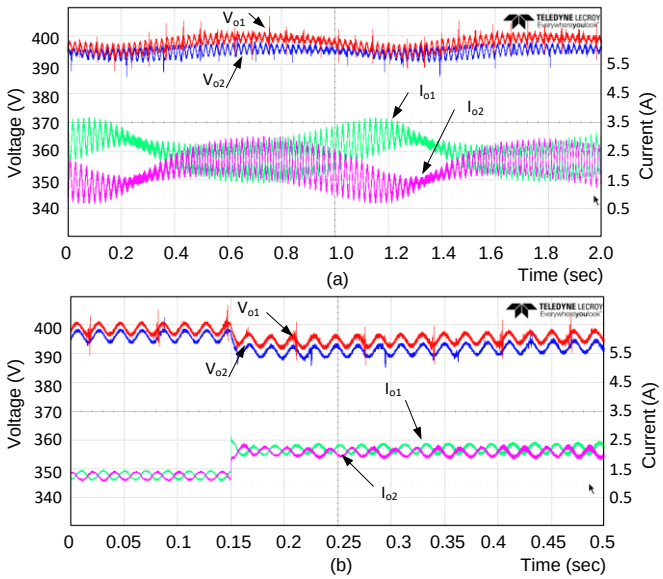

Fig. 17. Experimental results of (a) frequency droop control in [22], (b) adaptive droop approach, $I_{n,1} = I_{n,2}$, $d_{f1} = d_{f2} = 0.3$, $d_q = 25$, $R_{d1} = R_{d2} = 5\ \Omega$, $R_1 = 0\ \Omega$, $R_2 = 1.5\ \Omega$, and $V^* = 400\ V$.

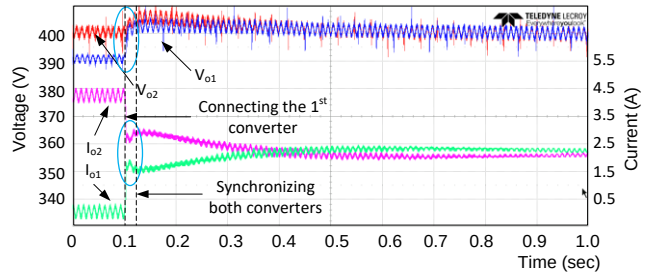

Fig. 18. Experimental results of Synchronization of the adaptive droop approach with equal converter ratings, $I_{n,1} = I_{n,2}$, $d_{f1} = d_{f2} = 0.3$, $d_q = 25$, $R_{d1} = R_{d2} = 5\ \Omega$, $R_1 = 1.5\ \Omega$, $R_2 = 2\ \Omega$, and $V^* = 400\ V$.

VI. Conclusion

In this paper, an adaptive droop controller is presented for the primary and secondary power sharing in LVDC microgrids based on a superimposed frequency. Both the primary and secondary layers fulfill the power sharing objectives by utilizing the local voltage, current and superimposed frequency information without employing an extra communication network, which implies a higher reliability compared to the communication-based power sharing approaches. The output current of the converters are accurately proportional to the rated current of converters, and output voltage of converters are regulated close to the reference value. The small signal model of the suggested control system for a simplified dc microgrid is obtained and its stability is analyzed in order to design the control parameters. The viability of the proposed control approach is ensured for equal and unequal DG ratings and different line impedances as well as for resistive and constant power loads. The proposed approach is verified by simulations and experimental tests.

Appendix

Effect of Superimposed AC Voltage on DC Loads

In this section, the effect of the superimposed ac voltage on dc loads are studied by employing the dynamic model of

loads. Modeling different types of loads is out of scope of this paper, hence the most common loads of a dc grid, i.e., constant power loads (converter-based) are considered in this section. The dynamic model of a dc/dc converter can be shown as Fig. 19 with double voltage and current regulators, where $G_v(s)$ and $G_i(s)$ are the voltage and current controllers, $G_{vg}(s)$, $G_{vd}(s)$, $G_{id}(s)$ and $G_{ig}(s)$ are the input to output, control to output, input to inductor current and control to inductor current transfer functions [37]. The transfer functions modeling the converter dynamic behavior are presented in [37].

In order to show the effect of the ac ripple superimposed to the input voltage, the closed loop transfer function from the input to output voltage (or inductor current) should be analyzed. From Fig. 19, the closed loop input voltage (V_{in}) to output voltage (V_{out}) transfer function ($H(s)$) can be calculated as:

$$H(s)=\frac{V_{out}}{V_{in}}=\frac{\dfrac{G_{ig}G_i}{(1+G_iG_{id})G_{vd}}+G_{vg}}{1+T_L}. \quad (27)$$

$$T_L=G_vG_iG_{vd}/(1+G_iG_{id})$$

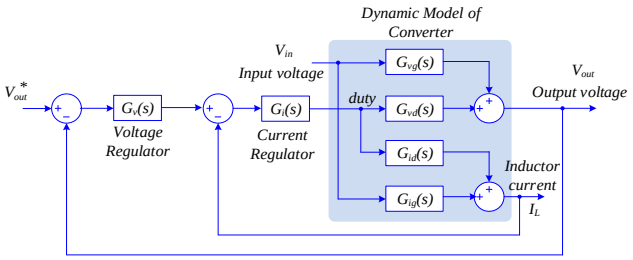

Fig. 19. Dynamic model and control block diagram of a dc/dc converter with voltage and current regulators.

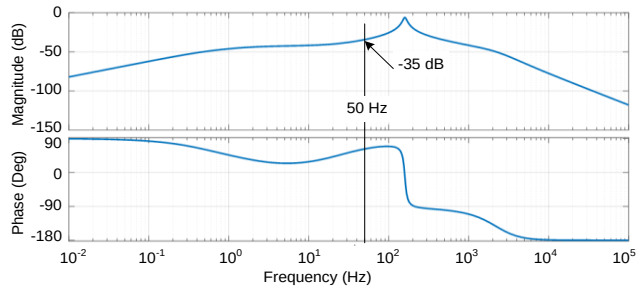

Fig. 20. Input to output transfer function (V_{out}/V_{in}) of a dc/dc buck converter – L_{dc} = 2 *mH*, C_{dc} = 500 μF, P_{out} = 2 *kW*, V_{in} = 400 *V*, V_{out} = 200 *V*, $G_v(s)$ = 5 + 20/s and $G_i(s)$ = 0.1 + 1/s.

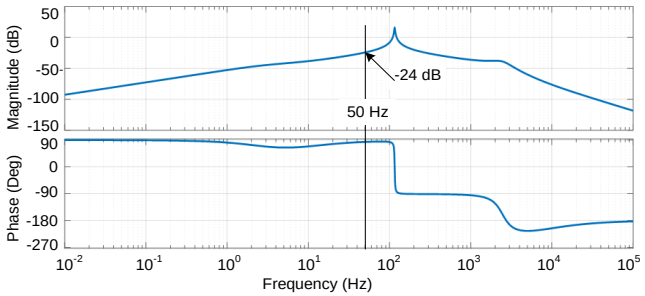

Fig. 21. Input to output transfer function (V_{out}/V_{in}) of a dc/dc boost converter – L_{dc} = 2 *mH*, C_{dc} = 500 μF, P_{out} = 2 *kW*, V_{in} = 400 *V*, V_{out} = 550 *V*, $G_v(s)$ = 2 + 20/s and $G_i(s)$ = 0.05 + 1/s.

According to [37], the loop transfer function $T_L(s)$ causes small gains at low frequencies. Therefore, the effect of input voltage ripple on the system dynamics will be rejected by the closed loop control system. For instance, $H(s)$ is shown in frequency domain for a conventional buck and boost converters in Fig. 20 and Fig. 21 respectively. The amplitude of $H(s)$ is very small at low frequencies, and for example, at 50 Hz, it is –35 *dB* for buck and –24 *dB* for boost converter. Therefore, at low frequencies, the effect of input voltage ripple and disturbances can be rejected by the closed loop control system. Moreover, the superimposed ac voltage in this paper is very small, i.e., 2.5 *V*, and it cannot affect the load dynamic behavior.

REFERENCES

[1] B. T. Patterson, "DC, Come Home: DC Microgrids and the Birth of the 'Enernet,'" *IEEE Power Energy Mag.*, vol. 10, no. 6, pp. 60–69, 2012.

[2] D. Boroyevich, I. Cvetkovic, R. Burgos, and D. Dong, "Intergrid: A Future Electronic Energy Network?," *IEEE J. Emerg. Sel. Top. Power Electron.*, vol. 1, no. 3, pp. 127–138, 2013.

[3] P. Fairley, "DC Versus AC: The Second War of Currents Has Already Begun [In My View]," *IEEE Power Energy Mag.*, vol. 10, no. 6, pp. 104–103, Nov. 2012.

[4] V. Nasirian, A. Davoudi, F. L. Lewis, and J. M. Guerrero, "Distributed Adaptive Droop Control for Dc Disribution Systems," *IEEE Trans. Energy Convers.*, vol. 29, no. 4, pp. 944–956, 2014.

[5] S. Moayedi and A. Davoudi, "Distributed Tertiary Control of DC Microgrid Clusters," *IEEE Trans. Power Electron.*, vol. 31, no. 2, pp. 1717–1733, 2015.

[6] Q. Shafiee, T. Dragicevic, J. C. Vasquez, and J. M. Guerrero, "Hierarchical Control for Multiple DC-Microgrids Clusters," *IEEE Trans. Energy Convers.*, vol. 29, no. 4, pp. 922–933, 2014.

[7] T. Dragicevic, J. M. Guerrero, J. C. Vasquez, and D. Skrlec, "Supervisory Control of an Adaptive-Droop Regulated DC Microgrid with Battery Management Capability," *IEEE Trans. Power Electron.*, vol. 29, no. 2, pp. 695–706, 2014.

[8] S. Anand, B. G. Fernandes, and J. M. Guerrero, "Distributed Control to Ensure Proportional Load Sharing and Improve Voltage Regulation in Low-Voltage DC Microgrids," *IEEE Trans. Power Electron.*, vol. 28, no. 4, pp. 1900–1913, 2013.

[9] J. M. Guerrero, J. C. Vasquez, J. Matas, L. G. De Vicuña, and M. Castilla, "Hierarchical Control of Droop-Controlled AC and DC Microgrids - A General Approach toward Standardization," *IEEE Trans. Ind. Electron.*, vol. 58, no. 1, pp. 158–172, 2011.

[10] S. Peyghami, H. Mokhtari, and F. Blaabjerg, "Hierarchical Power Sharing Control in DC Microgrids," in *Microgrid: Advanced Control Methods and Renewable Energy System Integration*, First., Magdi S Mahmoud, Ed. Elsevier Science & Technology, 2017, pp. 63–100.

[11] S. Peyghami-Akhuleh, H. Mokhtari, P. C. Loh, and F. Blaabjerg, "Distributed Secondary Control in DC Microgrids with Low-Bandwidth Communication Link," in *Proc IEEE PEDSTC*, 2016, pp. 641–645.

[12] D. Chen, L. Xu, and L. Yao, "DC Voltage Variation Based Autonomous Control of DC Microgrids," *IEEE Trans. Power Deliv.*, vol. 28, no. 2, pp. 637–648, 2013.

[13] A. Khorsandi, M. Ashourloo, and H. Mokhtari, "A Decentralized Control Method for a Low-Voltage DC Microgrid," *IEEE Trans. Energy Convers.*, vol. 29, no. 4, pp. 793–801, 2014.

[14] D. Chen and L. Xu, "Autonomous DC Voltage Control of a DC Microgrid with Multiple Slack Terminals," *IEEE Trans. Power Syst.*, vol. 27, no. 4, pp. 1897–1905, Nov. 2012.

[15] X. Lu, J. M. Guerrero, K. Sun, and J. C. Vasquez, "An Improved Droop Control Method for DC Microgrids Based on Low Bandwidth Communication With DC Bus Voltage Restoration and Enhanced Current Sharing Accuracy," *IEEE Trans. Power Electron.*, vol. 29, no. 4, pp. 1800–1812, Apr. 2014.

[16] D. Perreault, R. Selders, and J. Kassakian, "Frequency-Based Current-Sharing Techniques for Paralleled Power Converters," *IEEE Trans. Power Electron.*, vol. 13, no. 4, pp. 626–634, 1998.

[17] M. Angjelichinoski, C. Stefanovic, P. Popovski, H. Liu, P. C. Loh, and F. Blaabjerg, "Multiuser Communication through Power Talk in DC MicroGrids," *IEEE J. Sel. Areas Commun.*, vol. 34, no. 7, pp. 2006–2021, Jul. 2015.

[18] T. Dragičević, J. Guerrero, and J. C. Vasquez, "A Distributed Control Strategy for Coordination of an Autonomous LVDC Microgrid Based on Power-Line Signaling," *IEEE Trans. Ind. Electron.*, vol. 61, no. 7, pp. 3313–3326, 2014.

[19] A. Tuladhar, H. Jin, T. Unger, and K. Mauch, "Control of Parallel Inverters in Distributed AC Power Systems with Consideration of Line Impedance Effect," *IEEE Trans. Ind. Appl.*, vol. 36, no. 1, pp. 131–138, 2000.

[20] A. Tuladhar, H. Jin, T. Unger, and K. Mauch, "Parallel Operation of Single Phase Inverter Modules with No Control Interconnections," in *Proc. IEEE APEC*, 1997, vol. 1, pp. 94–100.

[21] A. Tuladhar and H. Jin, "A Novel Control Technique to Operate DC/DC Converters in Parallel with No Control Interconnections," in *Proc. IEEE PESC*, 1998, vol. 1, pp. 892–898.

[22] S. Peyghami, H. Mokhtari, P. C. Loh, P. Davari, and F. Blaabjerg, "Distributed Primary and Secondary Power Sharing in a Droop-Controlled LVDC Microgrid with Merged AC and DC Characteristics," *IEEE Trans. Smart Grid*, pp. 1–1, 2016.

[23] S. Peyghami, P. Davari, H. Mokhtari, P. C. Loh, and F. Blaabjerg, "Synchronverter-Enabled DC Power Sharing Approach for LVDC Microgrids," *IEEE Trans. Power Electron.*, pp. 1–1, 2016.

[24] Q. Shafiee, J. M. Guerrero, and J. C. Vasquez, "Distributed Secondary Control for Islanded Microgrids—A Novel Approach," *IEEE Trans. Power Electron.*, vol. 29, no. 2, pp. 1018–1031, 2014.

[25] T.-F. Wu, Y.-K. Chen, and Y.-H. Huang, "3C Strategy for Inverters in Parallel Operation Achieving an Equal Current Distribution," *IEEE Trans. Ind. Electron.*, vol. 47, no. 2, pp. 273–281, Apr. 2000.

[26] G. Ding, F. Gao, S. Zhang, P. C. Loh, and F. Blaabjerg, "Control of Hybrid AC / DC Microgrid under Islanding Operational Conditions," *J. Mod. Power Syst. Clean Energy*, vol. 2, no. 3, pp. 223–232, 2014.

[27] N. Hatziargyriou, H. Asano, R. Iravani, and C. Marnay, "Microgrids," *IEEE Power Energy Mag.*, vol. 5, no. 4, pp. 78–94, 2007.

[28] X. Lu, J. M. Guerrero, K. Sun, J. C. Vasquez, R. Teodorescu, and L. Huang, "Hierarchical Control of Parallel AC-DC Converter Interfaces for Hybrid Microgrids," *IEEE Trans. Smart Grid*, vol. 5, no. 2, pp. 683–692, 2014.

[29] J. M. Guerrero, L. Hang, and J. Uceda, "Control of Distributed Uninterruptible Power Supply Systems," *IEEE Trans. Ind. Electron.*, vol. 55, no. 8, pp. 2845–2859, 2008.

[30] J. Rocabert, A. Luna, F. Blaabjerg, and P. Rodriguez, "Control of Power Converters in AC Microgrids," *IEEE Trans. Power Electron.*, vol. 27, no. 11, pp. 4734–4749, 2012.

[31] M. Karimi-Ghartemani, "Universal Integrated Synchronization and Control for Single-Phase DC/AC Converters," *IEEE Trans. Power Electron.*, vol. 30, no. 3, pp. 1544–1557, 2015.

[32] S. Khongkhachat, "Hierarchical Control Strategies in AC Microgrids," 2015.

[33] P. C. Loh, D. Li, Y. K. Chai, and F. Blaabjerg, "Autonomous Control of Interlinking Converter with Energy Storage in Hybrid AC-DC Microgrid," *IEEE Trans. Ind. Appl.*, vol. 49, no. 3, pp. 1374–1382, 2013.

[34] Q. Zhong and G. Weiss, "Synchronverters: Inverters That Mimic Synchronous Generators," *IEEE Trans. Ind. Electron.*, vol. 58, no. 4, pp. 1259–1267, Apr. 2011.

[35] H. Nikkhajoei and R. Iravani, "Steady-State Model and Power Flow Analysis of Electronically-Coupled Distributed Resource Units," *IEEE Power Eng. Soc. Gen. Meet. PES*, vol. 22, no. 1, pp. 721–728, Jan. 2007.

[36] J. M. Guerrero, L. GarciadeVicuna, J. Matas, M. Castilla, and J. Miret, "Output Impedance Design of Parallel-Connected UPS Inverters With Wireless Load-Sharing Control," *IEEE Trans. Ind. Electron.*, vol. 52, no. 4, pp. 1126–1135, Aug. 2005.

[37] R. Erickson and D. Maksimovic, "*Fundamentals of Power Electronics*," Second. New York: Kluwer, 2001.

Saeed Peyghami (S'14) was born in Tabriz, Iran, in 1988. He received the B.Sc. and M.Sc. degrees both in electrical engineering from the Department of Electrical Engineering, Sharif University of Technology, Tehran, in 2010 and 2012, respectively. He is currently working toward the Ph.D. degree in electrical engineering at Sharif University of Technology, Tehran, Iran.

His research interests include power electronics system control, power quality, application of power electronics in distributed power systems.

Hossein Mokhtari (M'03–SM'14) was born in Tehran, Iran, on August 19, 1966. He received the B.Sc. degree in electrical engineering from Tehran University, Tehran, in 1989. He received the M.Sc. degree in power electronics from the University of New Brunswick, Fredericton, NB, Canada, in 1994, and the Ph.D. degree in power electronics/power quality from the University of Toronto, Toronto, ON, Canada in 1999.

From 1989 to 1992, he worked in the Consulting Division of Power Systems Dispatching Projects, Electric Power Research Center Institute, Tehran. Since 2000, he has been with the Department of Electrical Engineering, Sharif University of Technology, Tehran, where he is currently a Professor. He is also a Senior Consultant to several utilities and industries.

Frede Blaabjerg (S'86–M'88–SM'97–F'03) was with ABB-Scandia, Randers, Denmark, from 1987 to 1988. From 1988 to 1992, he was a Ph.D. Student with Aalborg University, Aalborg, Denmark. He became an Assistant Professor in 1992, Associate Professor in 1996, and Full Professor of power electronics and drives in 1998. His current research interests include power electronics and its applications such as in wind turbines, PV systems, reliability, harmonics and adjustable speed drives.

He has received 17 IEEE Prize Paper Awards, the IEEE PELS Distinguished Service Award in 2009, the EPE-PEMC Council Award in 2010, the IEEE William E. Newell Power Electronics Award 2014 and the Villum Kann Rasmussen Research Award 2014. He was an Editor-in-Chief of the IEEE TRANSACTIONS ON POWER ELECTRONICS from 2006 to 2012. He is nominated in 2014 and 2015 by Thomson Reuters to be between the most 250 cited researchers in Engineering in the world.